Active site conformational fluctuations promote the enzymatic activity of NDM-1

Hongmin Zhang[a#], Guixing Ma[a], Yifan Zhu[a], Lingxiao Zeng[b], Ashfaq Ahmad[a], Changzhi Wang[a], Bo Pang[b], Huiyan Fang[c], Liqing Zhao[c], Quan Hao[b#]

[a]Department of Biology, Guangdong Provincial Key Laboratory of Cell Microenvironment and Disease Research, Shenzhen Key Laboratory of Cell Microenvironment and SUSTech-HKU joint laboratories for matrix biology and diseases, Southern University of Science and Technology, Shenzhen 518055, China

[b]School of Biomedical Sciences, The University of Hong Kong, Hong Kong SAR, China

[c]College of Chemistry and Environmental Engineering, Shenzhen University, Shenzhen, Guangdong 518060, China

Running title：*Conformational fluctuation promotes enzymatic turnover*

#Correspondence should be addressed to Prof. Hongmin Zhang (email: zhanghm@sustc.edu.cn or hongmin_zhang@foxmail.com) or Prof. Quan Hao (email: qhao@hku.hk)

Keywords: microbial antibiotics resistance, metallo-beta-lactamase, NDM-1, conformational change, structure-based drug design

Abstract

Beta-lactam antibiotics are the mainstay for the treatment of bacterial infections. However, elevated resistance to these antibiotics mediated by metallo-β-lactamases (MBL) has become a global concern. New Delhi metallo-β-lactamase-1 (NDM-1), a newly added member of the MBL family that can hydrolyze almost all β-lactam antibiotics, has rapidly spread all over the world and posed serious clinical threats. Broad-spectrum and mechanism-based inhibitors against all MBLs are highly desired, but the differential mechanisms of MBLs towards different antibiotics pose a great challenge. To facilitate the design of mechanism-based inhibitors, we investigated the active-site conformational changes of NDM-1 through the determination of a series of 15 high-resolution crystal structures in native form and in complex with products, biochemical and biophysical studies, site-directed mutagenesis and molecular dynamics computation. The structural studies reveal the consistency of the active site conformations in NDM-1/products complexes and the fluctuation in native NDM-1 structures. The enzymatic measurements indicate a correlation between enzymatic activity and the active site fluctuation with more fluctuation favoring higher activity. This correlation is further validated by structural and enzymatic studies of the Q123G mutant. Our combinational studies suggest that active site conformational fluctuation promotes the enzymatic activity of NDM-1, which may guide further mechanism studies and inhibitor design.

Introduction

Beta-lactam antibiotics, including penicillins, cephalosporins and carbapenenms, constitute more than half of the antibiotics prescribed in clinical settings(1). However, the efficiency of these antibiotics is being continuously challenged by the emergence of resistant pathogenic bacteria, among which resistance to carbapenems is of extreme concern for that carbapenems are considered as the last resort for multidrug resistant infections. Beta-lactamases, which inactivate β-lactam antibiotics through hydrolyzing the β-lactam bonds(2), play a major role in antibiotic resistance(3, 4). Based on sequence similarity, β-lactamases can be divided into four classes (A, B, C and D)(5). Enzymes in classes A, C and D are serine-β-lactamases which harbor a serine residue at the active site to facilitate catalysis. And members of class B are metallo-β-lactamases (MBLs) that retain one or two zinc ions at the active site to facilitate β-lactam cleavage. MBLs are broad-spectrum β-lactamases, active against almost all β-lactams including carbapenems and even the clinically used inhibitors of serine-β-lactamases(6). Furthermore, most of the circulating MBLs are encoded in a transferable plasmid which may be rapidly disseminated in different strains and even different species of bacteria through horizontal gene transfer(7). For example, New Delhi metallo-β-lactamase-1 (NDM-1) is a newly added member of the MBL B1 subclass and since its first identification in 2009(8), NDM-1 positive bacteria have been identified in all continents except Antarctica(9).

NDM-1 shows broad activity at all β-lactam antibiotics except monobactams(8). Because of its rapid dissemination not only in clinical settings but also in community environments(10, 11), NDM-1 positive bacteria have posed a serious threat to our health care system. Since it identification in 2009, much effort has been put on the biochemical characterization(12-15), structural and mechanical studies(16-30), and inhibitor screening(31-35). It is highly desirable to find some potent specific inhibitors for NDM-1 or even broad-spectrum

inhibitors for all MBLs. However, because of the structural diversity of MBL active sites, the continuous evolving of these enzymes and the fact that very few residues are tightly constrained by function, the design of broad-spectrum MBL inhibitors is very challenging(6). Therefore, the design of MBL inhibitors may be best achieved by mimicking the focused nature of interactions observed in both substrate recognition and the catalytic mechanism(6) as in the case of serine β-lactamases. Unfortunately, the catalytic mechanism of NDM-1 is subtle and some detailed roles of active site residues are still under debate, such as substrate coordination(23, 26, 36), the individual roles of the two zinc ions, the identity and source of hydroxide for nucleophilic attack(16, 23, 26, 27), the protonation of β-lactam nitrogen after C-N bond cleavage(16, 23, 26) and the source of the next hydroxide for enzymatic turnover(23, 26) etc. Recent spectroscopic and structural investigations made significant progresses in the mechanism study of MBLs, but did not get to a consistent conclusion on the hydrolysis of carbapenems by NDM-1(29, 37), suggesting further study for the sake of mechanism-based broad-spectrum inhibitor design.

In this work, we investigated the conformational changes of the active site through the combination of crystallography, site-directed mutagenesis, enzymatic measurements and in silico simulation. Our results indicate a dynamic active site and its conformational fluctuation promotes the enzymatic activity of NDM-1, which may guide future inhibitor design.

Results

NDM-1 in complex with hydrolyzed antibiotics

In our previous study(16), we solved the first NDM-1 structure in complex with a hydrolyzed ampicillin and noticed that the distance between the two zinc ions at the active site was 4.6 Å, which was much longer than those of other MBLs. We proposed that this longer distance might correlate to the relatively lower enzymatic activity of NDM-1

compared to other B1 MBLs(16). And hence the longer distance might be an intrinsic property of NDM-1 in the product binding state. However, there is also a possibility of being a crystallographic artifact. To clarify if this longer distance is an intrinsic product binding property or crystallographic artifact, we determined a series of NDM-1/Amp structures at different crystallization conditions. As showed in Table 1, we re-crystallized NDM-1 in complex with ampicillin at the same condition as our previously reported one and got the highest resolution NDM-1/product structures up to now (1.00 Å). While the improvement of resolution revealed more accurate details, we noticed that the new structures were almost identical to that of previously solved one at the active site (Figure 1A). We further compared the structures determined from crystals in different conditions, such as different pHs and different precipitants. As shown by the first four structures in Table 1, although they were crystallized in different pHs and even in high salt, the structures are almost identical and can be superimposed with rmsd values ranging from 0.1 to 0.26 Å for all visible Cα atoms (Figure S1A for overall structure superposition). And besides overall structures, the active site confirmations of these structures are also very consistent with that of previously solved one with the Zn1-Zn2 distances ranging from 4.57 to 4.61 Å in 8 NDM-1 molecules, the distances of Zn1-OH and OH-Zn2 averaged at 2.00 ± 0.05 Å and 3.01 ± 0.04 Å (Figure 1B), respectively.

After our first report of NDM-1/Amp structure, several structures of NDM-1 in complex with other hydrolyzed antibiotics were also reported as listed in Table 1. For these structures of NDM-1 in complex with methicillin (4EY2)(22), oxacillin (4EYB)(22), benzylpenicillin (4EYF)(22), cephalexin (4RL2)(27) and ampicillin (4H0D(23), 4HL2(23) and 4RAW), the overall structures are very similar with rmsd values ranging from 0.10 to 0.36 Å for all the superimposed Cα atoms (Figure S1B). And for the active sites of these structures, Zn1-Zn2 distances were ranging from 4.48 to 4.63 Å (average value of 4.56 ± 0.05) while the distances

of Zn1-OH and OH-Zn2 were 1.98 ± 0.07 Å and 2.96 ± 0.10 Å (Figure S2A), respectively. The active site conformations observed in these structures are almost identical to those determined in our studies.

However, for structures of NDM-1 in complex with hydrolyzed meropenem (4EYL(22), 5N0H and 4RBS), the Zn1-Zn2 distances were a little bit shorter (ranging from 3.83 to 4.05 Å with an average 3.96 ± 0.09 Å). Inspection of these structures revealed that the hydrolyzed meropenem did not bind the active site like other hydrolyzed antibiotics (Figure S2A) with either the newly generated carboxylate group intercalating between the two zinc ions (4EYL and 5N0H) or the side ring carboxylate group not coordinated to Zn2 (4EYL and 4RBS) (Figure S2B). The intercalated conformation might be a rare binding state during product release, which was also suggested from the QM/MM calculation(38) as a rare inhibition state.

The structure of NDM-1 in complex with a reaction intermediate of cefuroxime (4RL0(27)) showed shorter Zn1-Zn2 distances (3.81/3.83 Å for two monomers) and OH-Zn2 distances (2.16/2.17 Å for two monomers). Active site inspection revealed that the newly generated carboxylate group did not coordinate to Zn1 as other products did. The shorter distance observed in this structure might be attributed to the reaction intermediate which needs further investigation.

Overall, in all NDM-1 structures with the hydrolyzed antibiotics coordinated to the active site in a product binding state, the Zn1-Zn2, Zn1-OH and OH-Zn2 distances are very consistent to be 4.6, 2.0 and 3.0 Å, respectively. This conformation should be an intrinsic NDM-1/product binding state and not a crystallographic artifact.

NDM-1 in native form

Since the identification of NDM-1 in 2009, many structures of NDM-1 in native form and in complex with antibiotics have been solved. Some of the reported structures showed no metal, mono metal(19) or not properly coordinated residue-metal interactions at the active

site(39). A Zn-Cd substituted NDM-1(20) (PDB 3ZR9) was obtained at pH7.5 with the Zn-Cd distance of 3.64 Å. While another structure(18) (PDB 3SPU) obtained at pH8.5 reported 5 molecules in the asymmetric unit and the Zn1-Zn2 distances ranging from 3.56 to 3.97 Å. It was then proposed that the Zn1-Zn2 distance was affected by different pHs(23). To reveal a clear and more accurate active site of native NDM-1 and what kind of factors can affect the active site conformation, we determined a series of native NDM-1 structures in different conditions including crystal packing, buffer components and pH variations.

Effect of crystal packing

In our search for native NDM-1 crystallization conditions, two crystal forms were obtained with form 1 retaining one molecule in the asymmetric unit and diffracted up to 0.95 Å resolution while form 2 harboring two molecules and diffracted between 1.05 and 1.55 Å depending on the crystallization precipitants (Table 2). For crystals of form 2, although they were obtained in different pHs and different buffer components (HEPES pH7.0 and pH7.5, imidazole pH7.5 and Tris pH8.0), the active site conformations are strikingly identical (Figure 2A and Figure S3) with the Zn1-Zn2, Zn1-OH and OH-Zn2 distances of 3.39 to 3.43 Å, 1.93 to 2.11 Å and 1.95 to 2.13 Å, respectively (Table 2). The Zn1-Zn2 distance is also consistent with the one measured by extended X-ray absorption fine structure study (3.38Å) (21). However, when we compare the structures of NDM-1 in forms 1 and 2 obtained in the same buffer and pH (imidazole pH7.5, PDB 5ZGZ and 5ZH1), we noticed that the Zn1-Zn2 distance in form1 is 3.62 Å while in form 2 it is 3.41/3.42 Å. The only difference between these two crystals is crystal packing so that the Zn1-Zn2 distance is clearly affected by crystal packing.

Effect of buffer components

Next, we compared the structures of form1 obtained at pH7.5 but prepared with different buffer components (imidazole, Bis-Tris and succinate). Despite of being crystallized at the

same pH, these structures showed different Zn1-Zn2 distances of 3.62 Å in imidazole, 3.59/3.53 Å in succinate and 3.49 Å in Bis-tris (Table 2), respectively. Although the differences are subtle, they can be repetitively observed, indicating that different buffer components do affect the active site conformations.

Effect of different pHs

And then, we examined the pH effect on the active site of NDM-1. To avoid the buffer component effect, all the NDM-1 structures were determined in the same buffer component but at different pHs. The crystals could be easily obtained by seeding in Bis-Tris buffer at different pHs, but with unidentifiable electron density at the active site at a lower pH (probably Bis-Tris but cannot be clearly modelled). To avoid potential perturbation of Bis-Tris to the active site, we then optimized the crystallization in succinate buffer and got the crystals at pH 5.5, 6.5 and 7.5. Although in crystals at pH5.5 and 6.5, succinate was observed at the active site, it can be clearly modelled with one hydroxyl group coordinated to Zn2 and substituting an apical water. This kind of interaction did not affect the other coordination bonds at the active site (Figure S3). Comparison of structures in succinate at pH5.5, 6.5 and 7.5 (Figure 2B) depicted a prominent decrease of the Zn1-Zn2 distances from 3.95, 3.78 to 3.59 Å (Table 2). To further confirm this pH effect, crystals obtained at pH5.5 were soaked in the cryo-protectant at pH7.5, which yielded a structure with the Zn1-Zn2 distance changed from 3.95 to 3.53 Å, indicating a consistent pH effect on the active site. Besides the clear tendency of Zn1-Zn2 changes according to different pHs, we also observed the decrease of OH-Zn2 distance along with the pH increase which is consistent with the Zn1-Zn2 changes (Table 2). However, Zn1-OH distances remain almost identical in all crystals we obtained and reported by others (1.99 ± 0.07 Å). Although in some structures this hydroxide was modelled as a water molecule, the shorter distance with Zn1 in all the structures indicates it should be a hydroxide. Furthermore, QM/MM study showed that if a water molecule

coordinates between the two zinc ions, the distance of Zn1-Zn2 will be 5.6 Å(23), much longer than those of all currently observed active sites. And the observed shorter Zn1-OH distance is also consistent with the mostly accepted idea that this hydroxide is mainly activated by Zn1 and acts as a nucleophile during the C-N bond break of β-lactam hydrolysis.

MD simulations

The distance of Zn1-Zn2 observed in different NDM-1 structures was also assessed by in silico calculations. MD simulations starting from the enzyme/hydrolyzed ampicillin structures (PDB: 5ZGE, 5ZGP, 5ZGR) were run to compare with experimental results. The energy minimized structures in different pH states presented similar Zn1-Zn2 distances of 4.7 Å (pH 5.5), 4.7 Å (pH 6.2) and 4.8 Å (pH 7.3). These results are very close to the experimentally determined distance of 4.6 Å, and do not show pH-dependence. The differences of Zn1-Zn2 distance observed in native NDM-1 at different pHs were also supported by our molecular dynamics analyses. Energy minimization showed Zn1-Zn2 distances of 3.9 Å, 3.7 Å and 3.5 Å for native NDM-1 at pH5.5, 6.5 and 7.5, respectively. Despite of subtle differences, the changing tendency of Zn1-Zn2 distances is consistent with the experimentally observed values. Previous QM/MM studies also calculated the Zn1-Zn2 distance of 3.58 Å(12), 3.60 Å (23) or 3.62 Å(40) in native NDM-1 although pH values were not reported in these studies. We also modelled an intact ampicillin molecule into the active site of native NDM-1 and performed MD simulations at different pHs which presented Zn1-Zn2 distances of 4.8Å (pH5.5), 3.8Å (pH6.5) and 3.4Å (pH7.5), respectively. The consistent decrease of Zn1-Zn2 distance in NDM-1/ampicillin models along with pH increase is similar to that observed for native unbound NDM-1, and well correlates to the enzymatic activity of NDM-1 at different pH (discussed later).

Overall, our results reveal that the longer distance in enzyme/hydrolyzed penam or cephalosporin complexes is an intrinsic feature of NDM-1 and Zn1-Zn2 distance in native

enzyme is affected by crystal packing, pH and buffer components. Next, we examined if the Zn1-Zn2 distance variation affects the enzymatic activity of NDM-1.

Enzymatic study of NDM-1

We first measured the enzymatic activity of wild type NDM-1 at different pHs (5.5, 6.5 and 7.5) prepared all with succinate to avoid the influence of buffer components. Imipenem was used as the substrate and the kcat values of NDM-1 at pH5.5, 6.5 and 7.5 are1283, 2060 and 3960 S^{-1}, respectively, roughly 2-fold for each pH increase (K_M and $Kcat/K_M$ parameters are listed in Table 3). The same pattern of increase was also observed using a buffer prepared with Bis-Tris in our assays and in other reports(23) although the specific values are different depending on substrates and assay conditions. It is interesting to note that along with pH increase, the enzymatic activity increases while Zn1-Zn2 distance shortens. In general, buffer pH may affect enzyme activity through charge changes on residues at the active site which may influence all the steps involved in enzyme catalysis including substrate binding, intermediate formation and product release. The facts that almost identical zinc coordination bonds, in particular the Zn1-OH distances (1.99 ± 0.07 Å) and geometries are kept in all native structures obtained in different pHs (Table S3) and that identical product-enzyme interactions are also observed in structures at different pHs (Figure 1), indicate that charge effect on the active site residues might be very subtle or indirect. The only obvious conformational change observed in these native structures at different pHs is the Zn1-Zn2 distance variation. Through careful structural comparison, we notice that the Zn2 coordination residue H250 progressively pushes Zn2 toward the active center from low to high pH (Figure 2B). Residue H250 locates at the tip of loop 12 which is relatively mobile among the structures at different pHs and has several charged residues at the other end. Through this long range interaction, we speculate that pH may fine tune Zn2 position and hence affect the enzymatic activity of NDM-1.

Mutagenesis studies to modulate the enzymatic activity and active site conformation

To further validate this speculation and test if modulation of the Zn1-Zn2 distance may affect the enzyme activity, site-directed mutants of NDM-1were generated and their enzymatic activities were measured. To avoid possible perturbation of the active site coordination and substrate binding, only second shell residues of the active site were mutated. Through careful structural inspection, residues A121 and Q123 were selected for mutagenesis studies. While both A121F and Q123G showed lower enzymatic activities, only Q123G was successfully crystallized. As shown in Table 3, the Kcat value for the Q123G mutant was 686 s^{-1}, much lower than that of wild type NDM-1 with the same assay condition (1814 s^{-1}).

The active site flexibility of Q123G mutant was evaluated experimentally by measuring the Zn1-Zn2 distance in high resolution crystal structures. We have successfully got the structure of the Q123G mutant at pH7.5 in succinate buffer at the resolution of 1.2Å. The overall structure of Q123G superimposed well to that of wild type NDM-1 with rmsd value of 0.44 Å for all Cα atoms and only minor flexibility in L3 loop was observed (Figure 3A). The Q123G mutation did not perturb the active site conformations nor the interactions around Q123 in wild type NDM-1 (Figure 3B). The Zn1-Zn2 distance in the Q123G mutant was measured to be 3.84 Å, a value longer than that of wild type NDM-1 at pH7.5 (3.59/3.53Å) and near that of wild type NDM-1 at pH6.5 (3.78Å). The enzymatic activity of the Q123G mutant is much lower than that of wild type NDM-1 at pH7.5 but near the proportional value of NDM-1 at pH6.5. In our enzymatic assay, imipenem was used as substrate. Measuring from the recently published structure of NDM-1 in complex with imipenem(29), the side chain of residue Q123 makes no contacts with imipenem and therefore would not affect its binding with the active site nor the release of hydrolyzed product. The activity decrease of the Q123G mutant should be solely attributed to the increase of Zn1-Zn2 distance, validating

our notion that modulation of the Zn1-Zn2 distance will affect the enzymatic activity of NDM-1.

Discussion

As revealed in the crystallographic structures, the active site of NDM-1, especially the Zn1-Zn2, is in a dynamic or oscillation state, depending on the environmental factors such as crystal packing, pH and buffer components. This is also observed in a single crystal(18) (PDB 3SPU) where there are 5 molecules in the asymmetric unit with 5 different Zn1-Zn2 distances ranging from 3.56 to 3.97 Å. And our enzymatic assays clearly show that the Zn1-Zn2 distance correlates to the enzymatic activity of NDM-1 with shorter Zn1-Zn2 distance in native NDM-1 having higher enzymatic activity. Interestingly, the distances of Zn1-Zn2 in enzyme/product complexes are all at the same value of 4.6 Å. Thus, its relation to enzymatic activity can be conveyed that bigger fluctuation (shorter Zn1-Zn2 distance) will favor higher enzymatic activity, or in other words, the fluctuation of Zn1-Zn2 promotes the enzymatic activity of NDM-1. The oscillation of Zn1-Zn2 distance during the enzymatic turnover was observed in mechanism studies of the subclass B3 MBL L1(41) and QM/MM calculations of NDM-1(24, 36), but here we attributed for the first time that such oscillations affect enzymatic turnover.

In previous mutagenesis and structural study of another B1 MBL BCII, Vila and coworkers also noticed that the active site conformational changes correlated the enzymatic activity of BCII and proposed that fine tuning of Zn2 position was responsible for the activity change of BCII(42-44). Comparison among the wild type and mutant BCII structures shows that the Zn1-Zn2 distances in activity impaired BCII (BCII/HD, PDB code 2NYP), wild type BCII (4C09/1BCII) and activity enhanced BCII (M5, PDB code 3FCZ) are 4.73, 3.50/3.85 and 3.32 Å, respectively. The relationship between enzymatic activity and Zn1-Zn2 distance in BCII well supports our notions in NDM-1 with shorter Zn1-Zn2 distance favoring higher

activity. Although fine tuning of Zn2 position can also explain the structure-activity relationship, Zn1-Zn2 distance variation is more specific. Considering that Zn1 also contributes to the conformational changes albeit at a less extent than Zn2 (Figure 2B), Zn1-Zn2 distance variation seems more accurate to explain current observations.

It is well known that conformational fluctuations are essential for substrate binding, product release and even can be rate-limiting step in enzymatic reactions. However, the role of conformational fluctuation along the reaction pathway was not well recognized. In this study, through series of crystallographic, biochemical and biophysical studies and simulation analyses, we presented a dynamic active site of NDM-1which well correlates to its enzymatic activity and proved that conformational fluctuation of the active site facilitates the enzymatic reaction. This phenomenon was also observed in dihydrofolate reductase where conformational fluctuation of an active site loop enhances its activity(45). In contrast to the covalently bonded active site residues in dihydrofolate reductase, the conformational fluctuation of the active site in NDM-1 is mainly presented by two noncovalently bonded metal ions. The active site fluctuation may facilitate the enzyme to sample high-energy conformational substrates that are conductive to form the transition state and promote the enzymatic reaction(45). Our combinational studies reveal that modulation of the active site fluctuation do affect the enzymatic activity of NDM-1, which may provide clues for future inhibitor design. For example, Zn1-Zn2 fluctuation may be restricted to a certain state by coordinating chemicals like substrate analogues as shown in a recent study(32, 46).

In summary, through the combination of crystallographic determination, biochemical and biophysical measurements, site-directed mutagenesis and in silico simulation, our results reveal that: 1) the longer distance of Zn1-Zn2 (4.6 Å) in enzyme/product complex is an intrinsic feature of NDM-1; 2) the Zn1-Zn2 distance in native NDM-1 varies depending on external factors like crystal packing, pH and buffer components; 3) the variation of Zn1-Zn2

distance affects the enzymatic activity of NDM-1 with shorter distance favoring higher enzymatic activity.

Materials and Methods

Protein expression, purification and site-directed mutagenesis

Wild type *NDM-1* (G29-R270) was cloned into a His-MBP vector to facilitate protein folding and purification. The fusion construct was expressed in *E. coli* BL21 (DE3) and the cells were allowed to grown up to OD600 of 0.6 followed by induction of 0.5 mM IPTG overnight at 16 °C. After centrifugation, cell pellet was suspended in lysis buffer of 20 mM HEPES pH 7.4, 0.5 M sodium chloride for sonication. The supernatant was loaded to a nickel-NTA chromatography column (GE healthcare) and NDM-1 was purified by an imidazole gradient. Effluents from nickel column were further purified by a MBP column. The fusion tag was cleaved with TEV protease and separated from NDM-1 by passing through a Ni-NTA column again. NDM-1 was in the flow-through fraction and was further purified by a Q-sepharose ion exchange column (GE healthcare) at pH 7.0 with a sodium chloride gradient from 0 to 0.3 M. The purified protein was buffer-exchanged into 50 mM NaCl and concentrated to 100 mg/ml (measured at OD280 using an extinction coefficient of 27960) for later use.

For site-directed mutagenesis, wild type NDM-1 was used as the template and the mutations were introduced using the quick-change method. The mutants were confirmed by sequencing and the expression and purification of the mutant proteins were performed as same as that of wild type NDM-1.

Crystallization, diffraction data collection and structure refinement

Wild type NDM-1 crystals were screened by sitting drop vapor diffusion method. NDM-1 in complex with ampicillin crystals were observed in several conditions and were further optimized by hanging drop method. Crystals for native NDM-1 were obtained in two forms with form 1 having one molecule per asymmetric unit and form 2 having two molecules per asymmetric unit. The detailed crystallization and cryo-protection conditions were listed in Table S1. All crystals were cryo-protected and then flash frozen in liquid nitrogen. The diffraction data were collected at 100 K on station BL17U1 or BL19U1 at the Shanghai Synchrotron Radiation Facility and processed with

HKL2000(47). The structures were solved by molecular replacement method using the previously solved NDM-1/Amp complex(16) (PDB code 3Q6X) as searching model. The models were refined with Refmac(48, 49) in the CCP4 suite(50) and then cycled with rebuilding in Coot(51). TLS refinement(52) was incorporated into the later stages of the refinement process. Solvents were added automatically in Coot and then manually inspected and modified. The final models were analyzed with MolProbity(53) showing that almost all amino acid residues were in favored regions of the Ramachandran plot while residues D90 were in a forbidden region as noticed previously(16). Data collection and model refinement statistics for all datasets were summarized in **Table S2**. The coordinates and structure factors were deposited in the Protein Data Bank with entry codes also listed in **Table S2**.

Enzymatic activity measurement

Hydrolysis of antibiotics by wild type and mutant NDM-1were monitored by detecting a reduction in the absorbance that resulted from the opening of the β-lactam ring using imipenem as substrate(39). Activity for the pH dependence of wild type NDM-1 was measured in a reaction buffer containing 50 mM succinate (pH5.5, 6.5 or 7.5), 100 mM NaCl, 50 μM $ZnCl_2$, 10 μg/ml BSA, 50 nM NDM-1 and varying concentrations of imipenem. The comparison of enzymatic activity between wild type and mutant NDM-1 was assayed in a reaction buffer containing 50 mM HEPES (pH7.5), 100 mM NaCl, 100 μM $ZnCl_2$, 10 μg/ml BSA, 50 nM enzymes and varying concentrations of imipenem. All the experiments were performed at 25°C and the A300 value was immediately measured using a perkinelmer spectrophotometer enspire. Kinetic parameters were determined by plotting the initial velocities against substrate concentrations and curve fitting with the Graphpad prism5 software. All measurements were repeated three times and the average values were presented.

Simulation

The native models were taken from the crystal structures solved in succinate buffer at pH5.5, 6.5 and 7.5, respectively. The enzyme/product models were taken from structures solved at pH5.5 (PDB code 5ZGE), pH6.2 (5ZGP) and pH7.3 (5ZGR), respectively. NDM-1 in complex with hydrolyzed ampicillin was superimposed onto the native models. The

coordinates of hydrolyzed ampicillin were kept and the chemical structure was modified to generate the substrate ampicillin. Then we got the initial models of three enzyme-substrate systems at different pHs. All the water molecules, solvent and succinate molecules in crystal structures were removed from the initial models, and the shared coordination hydroxide was kept. Polar hydrogens were added to the systems using *H*++ web-server(54).

MD simulations were carried out using Amber 12(55). The script MCPB.py(56) was applied to generate parameters of the above models for further MD simulation. The ff14SB force field was used for the protein systems(57). Each model was then solvated in a periodic box surrounded by no less than 10 Å TIP3P water molecules(58). Counter ions were added to maintain neutral charge of systems. To remove possible poor contacts between the solute and solvent, energy minimizations using a combination of the steepest descent and conjugated gradient method was performed. For models with ampicillin, each system was subjected to a slow heating process for 500 ps from 0 to 300K and then was equilibrated for 500 ps under a NPT ensemble at a constant temperature of 300 K. Finally, production MD simulations were conducted for 20ns. The Sander program was used to conduct the MD simulation at constant temperature (300 K) and pressure (1.0 atm) with a time step of 1 fs. The non-bonded cutoff was set to 12.0 Å, and electrostatic interactions were calculated using the particle-mesh Ewald method(59). The SHAKE algorithm(60) was used to constrain bonds involving hydrogen atoms.

Supporting Information

Figure S1. Superposition of overall structures of NDM-1 in complex with hydrolyzed antibiotics. (file type, TIFF)

Figure S2. Active site conformations of NDM-1 in complex with hydrolyzed antibiotics. (file type, TIFF)

Figure S3. Superposition of the overall structures of native NDM-1 crystallized in form2. (file type, TIFF)

Figure S4. Active sites of native NDM-1 crystallized in succinate at pH5.5 and pH6.5. (file type, TIFF)

Table S1. Crystallization conditions and cryoprotectants for NDM-1 crystals. (file type, DOC)

Table S2. Data collection and refinement statistics. (file type, DOC)

Table S3. Active site coordination of wild type and mutant NDM-1. (file type, DOC)

Author contributions

HZ and QH designed the experiments. HZ and GM performed the crystallography work. YZ, CW, BP, HF and LZ performed the biochemical and biophysical assays. LZ and AA performed the computation work. HZ and QH wrote the manuscript. All authors approved the manuscript.

Acknowledgements

This work was supported by Natural Science Foundation of China grant (31670753 to HZ), Guangdong Science and Technology Program (2017B030301018 to HZ), research grants from Shenzhen Science and Technology Innovation Committee (JCYJ20160608140912962 and ZDSYS20140509142721429 to HZ), the Health and Medical Research Fund of Hong Kong (15140992 to QH), the Hong Kong RGC grants (C5026-16G and AoE/P-705/16 to QH), Natural Science Foundation of Guangdong Province (2016A030313053 to LZ) and the Special Fund for Development of Strategic Emerging Industries in Shenzhen (JCYJ20160520174823939 to LZ). We thank the staff from BL17U1 and BL19U1 beamlines at Shanghai Synchrotron Radiation Facility for technical support.

Conflict of interest

The authors declare that they have no conflicts of interest in the contents of this article.

References

1. Drawz SM, Bonomo RA. 2010. Three decades of beta-lactamase inhibitors. Clin Microbiol Rev 23:160-201.
2. Page MI. 1999. The reactivity of beta-lactams, the mechanism of catalysis and the inhibition of beta-lactamases. Curr Pharm Des 5:895-913.
3. Fisher JF, Meroueh SO, Mobashery S. 2005. Bacterial resistance to beta-lactam antibiotics: compelling opportunism, compelling opportunity. Chem Rev 105:395-424.
4. Llarrull LI, Testero SA, Fisher JF, Mobashery S. 2010. The future of the beta-lactams. Curr Opin Microbiol 13:551-7.
5. Bush K, Jacoby GA. 2010. Updated functional classification of beta-lactamases. Antimicrob Agents Chemother 54:969-76.
6. Mojica MF, Bonomo RA, Fast W. 2016. B1-Metallo-beta-Lactamases: Where Do We Stand? Curr Drug Targets 17:1029-50.
7. Johnson AP, Woodford N. 2013. Global spread of antibiotic resistance: the example of New Delhi metallo-beta-lactamase (NDM)-mediated carbapenem resistance. J Med Microbiol 62:499-513.
8. Yong D, Toleman MA, Giske CG, Cho HS, Sundman K, Lee K, Walsh TR. 2009. Characterization of a new metallo-beta-lactamase gene, bla(NDM-1), and a novel erythromycin esterase gene carried on a unique genetic structure in Klebsiella pneumoniae sequence type 14 from India. Antimicrob Agents Chemother 53:5046-54.
9. Lee CR, Lee JH, Park KS, Kim YB, Jeong BC, Lee SH. 2016. Global Dissemination of Carbapenemase-Producing Klebsiella pneumoniae: Epidemiology, Genetic Context, Treatment Options, and Detection Methods. Front Microbiol 7:895.
10. Walsh TR, Weeks J, Livermore DM, Toleman MA. 2011. Dissemination of NDM-1 positive bacteria in the New Delhi environment and its implications for human health: an environmental point prevalence study. Lancet Infect Dis 11:355-62.
11. Toleman MA, Bugert JJ, Nizam SA. 2015. Extensively drug-resistant New Delhi metallo-beta-lactamase-encoding bacteria in the environment, Dhaka, Bangladesh, 2012. Emerg Infect Dis 21:1027-30.
12. Thomas PW, Zheng M, Wu S, Guo H, Liu D, Xu D, Fast W. 2011. Characterization of purified New Delhi metallo-beta-lactamase-1. Biochemistry 50:10102-13.
13. Li T, Wang Q, Chen F, Li X, Luo S, Fang H, Wang D, Li Z, Hou X, Wang H. 2013. Biochemical characteristics of New Delhi metallo-beta-lactamase-1 show unexpected difference to other MBLs. PLoS One 8:e61914.
14. Chen J, Chen H, Shi Y, Hu F, Lao X, Gao X, Zheng H, Yao W. 2013. Probing the effect of the non-active-site mutation Y229W in New Delhi metallo-beta-lactamase-1 by site-directed mutagenesis, kinetic studies, and molecular dynamics simulations. PLoS One 8:e82080.

15. Marcoccia F, Bottoni C, Sabatini A, Colapietro M, Mercuri PS, Galleni M, Kerff F, Matagne A, Celenza G, Amicosante G, Perilli M. 2016. Kinetic Study of Laboratory Mutants of NDM-1 Metallo-beta-Lactamase and the Importance of an Isoleucine at Position 35. Antimicrob Agents Chemother 60:2366-72.
16. Zhang H, Hao Q. 2011. Crystal structure of NDM-1 reveals a common beta-lactam hydrolysis mechanism. FASEB J 25:2574-82.
17. Zheng B, Tan S, Gao J, Han H, Liu J, Lu G, Liu D, Yi Y, Zhu B, Gao GF. 2011. An unexpected similarity between antibiotic-resistant NDM-1 and beta-lactamase II from Erythrobacter litoralis. Protein Cell 2:250-8.
18. King D, Strynadka N. 2011. Crystal structure of New Delhi metallo-beta-lactamase reveals molecular basis for antibiotic resistance. Protein Sci 20:1484-91.
19. Kim Y, Tesar C, Mire J, Jedrzejczak R, Binkowski A, Babnigg G, Sacchettini J, Joachimiak A. 2011. Structure of apo- and monometalated forms of NDM-1--a highly potent carbapenem-hydrolyzing metallo-beta-lactamase. PLoS One 6:e24621.
20. Green VL, Verma A, Owens RJ, Phillips SE, Carr SB. 2011. Structure of New Delhi metallo-beta-lactamase 1 (NDM-1). Acta Crystallogr Sect F Struct Biol Cryst Commun 67:1160-4.
21. Yang H, Aitha M, Hetrick AM, Richmond TK, Tierney DL, Crowder MW. 2012. Mechanistic and spectroscopic studies of metallo-beta-lactamase NDM-1. Biochemistry 51:3839-47.
22. King DT, Worrall LJ, Gruninger R, Strynadka NC. 2012. New Delhi metallo-beta-lactamase: structural insights into beta-lactam recognition and inhibition. J Am Chem Soc 134:11362-5.
23. Kim Y, Cunningham MA, Mire J, Tesar C, Sacchettini J, Joachimiak A. 2013. NDM-1, the ultimate promiscuous enzyme: substrate recognition and catalytic mechanism. FASEB J 27:1917-27.
24. Zheng M, Xu D. 2013. New Delhi metallo-beta-lactamase I: substrate binding and catalytic mechanism. J Phys Chem B 117:11596-607.
25. Yang H, Young H, Yu S, Sutton L, Crowder MW. 2014. Targeting metallo-carbapenemases via modulation of electronic properties of cephalosporins. Biochem J 464:271-9.
26. Yang H, Aitha M, Marts AR, Hetrick A, Bennett B, Crowder MW, Tierney DL. 2014. Spectroscopic and mechanistic studies of heterodimetallic forms of metallo-beta-lactamase NDM-1. J Am Chem Soc 136:7273-85.
27. Feng H, Ding J, Zhu D, Liu X, Xu X, Zhang Y, Zang S, Wang DC, Liu W. 2014. Structural and mechanistic insights into NDM-1 catalyzed hydrolysis of cephalosporins. J Am Chem Soc 136:14694-7.
28. Das CK, Nair NN. 2017. Hydrolysis of cephalexin and meropenem by New Delhi metallo-beta-lactamase: the substrate protonation mechanism is drug dependent. Phys Chem Chem Phys 19:13111-13121.
29. Feng H, Liu X, Wang S, Fleming J, Wang DC, Liu W. 2017. The mechanism of NDM-1-catalyzed carbapenem hydrolysis is distinct from that of penicillin or cephalosporin hydrolysis. Nat Commun 8:2242.
30. Serag MF, Abadi M, Habuchi S. 2014. Single-molecule diffusion and conformational dynamics by spatial integration of temporal fluctuations. Nat Commun 5:5123.
31. Thomas PW, Cammarata M, Brodbelt JS, Fast W. 2014. Covalent inhibition of New Delhi metallo-beta-lactamase-1 (NDM-1) by cefaclor. Chembiochem 15:2541-8.

32. Gonzalez MM, Kosmopoulou M, Mojica MF, Castillo V, Hinchliffe P, Pettinati I, Brem J, Schofield CJ, Mahler G, Bonomo RA, Llarrull LI, Spencer J, Vila AJ. 2015. Bisthiazolidines: A Substrate-Mimicking Scaffold as an Inhibitor of the NDM-1 Carbapenemase. ACS Infect Dis 1:544-54.
33. Klingler FM, Wichelhaus TA, Frank D, Cuesta-Bernal J, El-Delik J, Muller HF, Sjuts H, Gottig S, Koenigs A, Pos KM, Pogoryelov D, Proschak E. 2015. Approved Drugs Containing Thiols as Inhibitors of Metallo-beta-lactamases: Strategy To Combat Multidrug-Resistant Bacteria. J Med Chem 58:3626-30.
34. Christopeit T, Leiros HK. 2016. Fragment-based discovery of inhibitor scaffolds targeting the metallo-beta-lactamases NDM-1 and VIM-2. Bioorg Med Chem Lett 26:1973-7.
35. Groundwater PW, Xu S, Lai F, Varadi L, Tan J, Perry JD, Hibbs DE. 2016. New Delhi metallo-beta-lactamase-1: structure, inhibitors and detection of producers. Future Med Chem 8:993-1012.
36. Zhu K, Lu J, Liang Z, Kong X, Ye F, Jin L, Geng H, Chen Y, Zheng M, Jiang H, Li JQ, Luo C. 2013. A quantum mechanics/molecular mechanics study on the hydrolysis mechanism of New Delhi metallo-beta-lactamase-1. J Comput Aided Mol Des 27:247-56.
37. Lisa MN, Palacios AR, Aitha M, Gonzalez MM, Moreno DM, Crowder MW, Bonomo RA, Spencer J, Tierney DL, Llarrull LI, Vila AJ. 2017. A general reaction mechanism for carbapenem hydrolysis by mononuclear and binuclear metallo-beta-lactamases. Nat Commun 8:538.
38. Yuan Q, He L, Ke H. 2012. A potential substrate binding conformation of beta-lactams and insight into the broad spectrum of NDM-1 activity. Antimicrob Agents Chemother 56:5157-63.
39. Guo Y, Wang J, Niu G, Shui W, Sun Y, Zhou H, Zhang Y, Yang C, Lou Z, Rao Z. 2011. A structural view of the antibiotic degradation enzyme NDM-1 from a superbug. Protein Cell 2:384-94.
40. Chen J, Chen H, Zhu T, Zhou D, Zhang F, Lao X, Zheng H. 2014. Asp120Asn mutation impairs the catalytic activity of NDM-1 metallo-beta-lactamase: experimental and computational study. Phys Chem Chem Phys 16:6709-16.
41. Breece RM, Hu Z, Bennett B, Crowder MW, Tierney DL. 2009. Motion of the zinc ions in catalysis by a dizinc metallo-beta-lactamase. J Am Chem Soc 131:11642-3.
42. Tomatis PE, Rasia RM, Segovia L, Vila AJ. 2005. Mimicking natural evolution in metallo-beta-lactamases through second-shell ligand mutations. Proc Natl Acad Sci U S A 102:13761-6.
43. Gonzalez JM, Medrano Martin FJ, Costello AL, Tierney DL, Vila AJ. 2007. The Zn2 position in metallo-beta-lactamases is critical for activity: a study on chimeric metal sites on a conserved protein scaffold. J Mol Biol 373:1141-56.
44. Tomatis PE, Fabiane SM, Simona F, Carloni P, Sutton BJ, Vila AJ. 2008. Adaptive protein evolution grants organismal fitness by improving catalysis and flexibility. Proc Natl Acad Sci U S A 105:20605-10.
45. Bhabha G, Lee J, Ekiert DC, Gam J, Wilson IA, Dyson HJ, Benkovic SJ, Wright PE. 2011. A dynamic knockout reveals that conformational fluctuations influence the chemical step of enzyme catalysis. Science 332:234-8.
46. Hinchliffe P, Gonzalez MM, Mojica MF, Gonzalez JM, Castillo V, Saiz C, Kosmopoulou M, Tooke CL, Llarrull LI, Mahler G, Bonomo RA, Vila AJ, Spencer J. 2016. Cross-class

metallo-beta-lactamase inhibition by bisthiazolidines reveals multiple binding modes. Proc Natl Acad Sci U S A 113:E3745-54.
47. Otwinowski Z, Minor W. 1997. Processing of X-ray diffraction data collected in oscillation mode. Methods in enzymology:307-325.
48. Murshudov GN, Vagin AA, Dodson EJ. 1997. Refinement of macromolecular structures by the maximum-likelihood method. Acta Crystallogr D Biol Crystallogr 53:240-55.
49. Murshudov GN, Skubak P, Lebedev AA, Pannu NS, Steiner RA, Nicholls RA, Winn MD, Long F, Vagin AA. 2011. REFMAC5 for the refinement of macromolecular crystal structures. Acta Crystallogr D Biol Crystallogr 67:355-67.
50. Collaborative Computational Project N. 1994. The CCP4 suite: programs for protein crystallography. Acta Crystallogr D Biol Crystallogr 50:760-3.
51. Emsley P, Lohkamp B, Scott WG, Cowtan K. 2010. Features and development of Coot. Acta Crystallogr D Biol Crystallogr 66:486-501.
52. Painter J, Merritt E. 2006. TLSMD web server for the generation of multi-group TLS models. Journal of Applied Crystallography 39:109-111.
53. Chen VB, Arendall WB, 3rd, Headd JJ, Keedy DA, Immormino RM, Kapral GJ, Murray LW, Richardson JS, Richardson DC. 2010. MolProbity: all-atom structure validation for macromolecular crystallography. Acta Crystallogr D Biol Crystallogr 66:12-21.
54. Anandakrishnan R, Aguilar B, Onufriev AV. 2012. H++3.0: automating pK prediction and the preparation of biomolecular structures for atomistic molecular modeling and simulations. Nucleic Acids Research 40:W537-W541.
55. Case DA, Darden TA, Cheatham III TE, Simmerling CL, Wang J, Duke RE, Luo R, Walker RC, Zhang W, Merz KM, Roberts S, Wang B, Hayik S, Roitberg A, Seabra G, Swails J, GÖtz AW, Kolossvary I, Wong KF, Paesani F, Vanicek J, Wolf RM, Liu J, Wu X, Brozell SR, Steinbrecher T, Gohlke H, Cai Q, Ye X, Wang J, Hsieh M-J, Hornak V, Cui G, Roe DR, Mathews DH, Seetin MG, Salomon-Ferrer R, Sagui C, Babin V, Luchko T, Gusarov S, Kovalenko A, Kollman PA. 2012. AMBER 12, University of California, San Francisco.
56. Li PF, Merz KM. 2016. MCPB.py: A Python Based Metal Center Parameter Builder. Journal of Chemical Information and Modeling 56:599-604.
57. Maier JA, Martinez C, Kasavajhala K, Wickstrom L, Hauser KE, Simmerling C. 2015. ff14SB: Improving the Accuracy of Protein Side Chain and Backbone Parameters from ff99SB. Journal of Chemical Theory and Computation 11:3696-3713.
58. Jorgensen WL, Chandrasekhar J, Madura JD, Impey RW, Klein ML. 1983. Comparison of Simple Potential Functions for Simulating Liquid Water. Journal of Chemical Physics 79:926-935.
59. Essmann U, Perera L, Berkowitz ML, Darden T, Lee H, Pedersen LG. 1995. A Smooth Particle Mesh Ewald Method. Journal of Chemical Physics 103:8577-8593.
60. Ryckaert JP, Ciccotti G, Berendsen HJC. 1977. Numerical-Integration of Cartesian Equations of Motion of a System with Constraints - Molecular-Dynamics of N-Alkanes. Journal of Computational Physics 23:327-341.

Figure legends

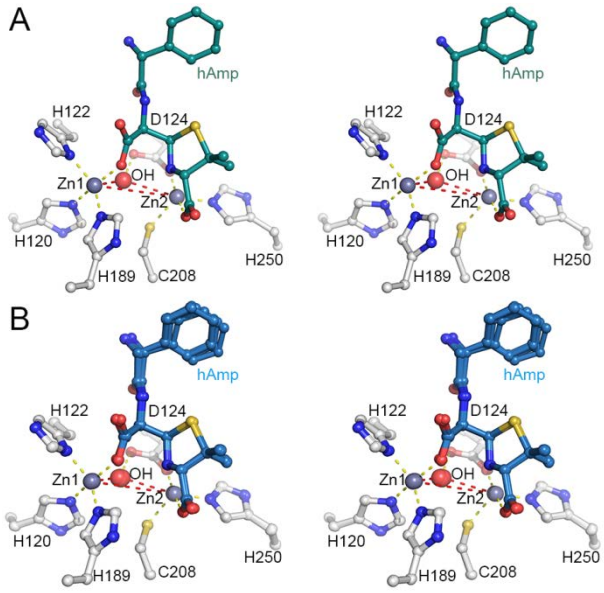

Figure 1. Active site conformation of NDM-1 in complex with hydrolyzed ampicillin crystallized at pH5.5 (A) and superposition of the active sites of NDM-1 crystallized at different conditions (B). Active site residues and hydrolyzed ampicillin were shown as ball-and-stick models. The residues were colored with grey carbons, the hydrolyzed ampicillin was colored with green and cyan carbons in (A) and (B), respectively. Zinc ions and hydroxide were shown as grey and red balls, respectively. Coordination bonds between zinc ions and active site residues were shown as yellow dash lines. The distances between Zn1-OH, OH-Zn2 and Zn1-Zn2 were 2.1, 3.0 and 4.6Å (shown as red dashed lines), respectively.

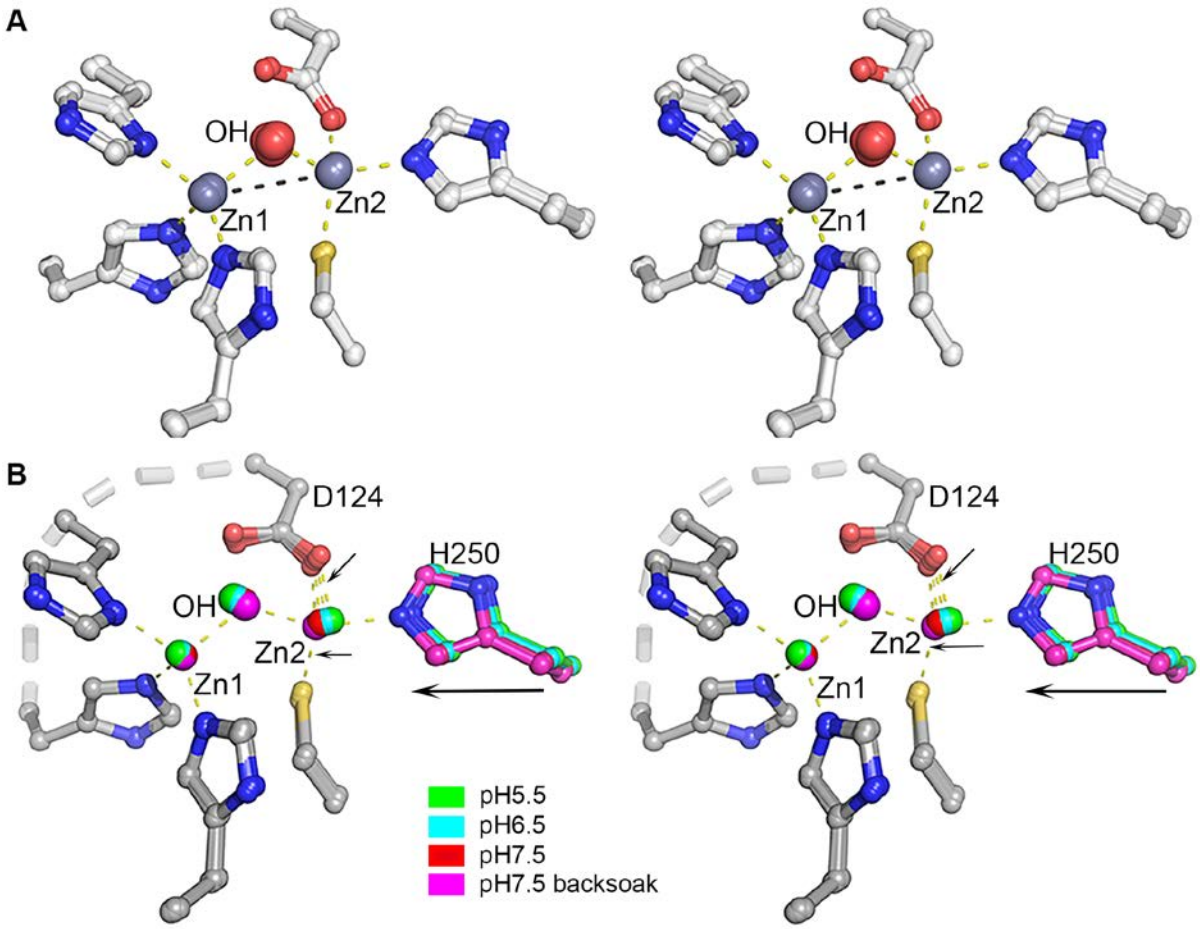

Figure 2. Active site conformations of native NDM-1. Active site residues were shown as ball-and-stick models while zinc ions and hydroxide at the active site were shown as spheres. Coordination bonds were shown as yellow dash lines. (A) Superposition of active sites of 8 native NDM-1 crystallized in form2. The active site conformations are strikingly identical among structures from different crystallization conditions, especially the Zn1-OH, OH-Zn2 and Zn1-Zn2 conformations and distances. (B) Superposition of active sites of native NDM-1 crystallized in form1 at pH5.5, 6.5 and 7.5 in succinate buffers. The zinc ions, hydroxide ion and carbon atoms in residue H250 were colored in green, cyan, red and magenta for crystals at pH5.5, 6.5, 7.5 and 7.5 (soaked at pH7.5 from crystals of pH5.5), respectively. Residue H250 pushes Zn2 to the active center along with pH increase. Residue D124 adjusts its side chain carboxylate group accordingly to coordinate to Zn2.

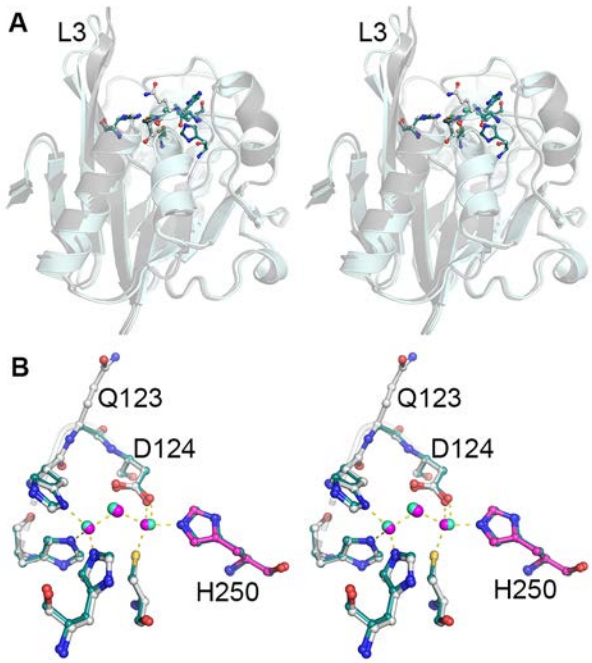

Figure 3. Structural comparison between wild type and Q123G mutant NDM-1. Q123G mutant NDM-1 was superimposed onto wild type NDM-1 (succinate, pH7.5, PDB code 5ZGW). Active site residues were shown as ball-and-stick models while zinc ions and hydroxide at the active site were shown as spheres. Coordination bonds were shown as yellow dash lines. (A) Overall structural superimposition. L3 loops show flexibility between these two structures. (B) Active sites superimposition. The zinc ions, hydroxide ion and carbon atoms in residue H250 were colored in cyan and magenta for Q123G and wild type NDM-1, respectively. Q123G mutation did not perturb the active site conformation obviously. The distance of Zn1-Zn2 in Q123G is longer than that in wild type NDM-1.

636

Table 1. NDM-1 in complex with hydrolysed products

PDB	Complex	Resolution (Å)	M1-M2 distance(Å)	M1-OH distance(Å)	OH-M2 dstance(Å)	Crystallization condition	Reference and remark
5ZGE	Ampicillin	1.00	4.60/4.61	2.08/2.09	2.98/2.94	0.1M Bis-Tris pH5.5, 0.2M Li_2SO_4, 25% PEG3350	This work
5ZGP	Ampicillin	1.15	4.59/4.59	1.97/1.94	2.99/3.04	0.1M Bis-Tris pH6.2, 0.2M Li_2SO_4, 15% PEG3350, 20 mg/ml ampicillin	This work
5ZGR	Ampicillin	1.15	4.59/4.59	1.98/1.99	3.01/3.04	0.1M HEPES pH7.3, 20% PEG3350, 20 mg/ml ampicillin	This work
5ZGQ	Ampicillin	1.50	4.58/4.57	1.99/1.97	3.04/3.04	0.1M Tris-HCl pH7.5, 25% PEG4000, 0.7M $(NH_4)_2SO_4$, 20mg/ml ampicillin	This work
4EY2	Methicillin	1.17	4.57/4.58	1.95/1.97	2.99/3.00	0.2M MgCl2, 25% PEG3350, 0.1M bis-tris pH5.5	(22)
4EYB	Oxacillin	1.16	4.54/4.55	1.98/1.96	2.94/2.98	0.2M MgCl2, 25% PEG3350, 0.1M bis-tris pH5.5	(22)
4EYF	Benzylpenicillin	1.8	4.63/4.61	1.98/1.93	3.11/3.08	0.2M MgCl2, 25% PEG3350, 0.1M bis-tris pH5.5	(22)
4RL2	Cefalexin	2.01	4.48/4.55	1.83/2.00	2.99/2.78	28% (w/v) PEG3350, 0.1 M Bis-Tris, pH 5.8, 0.2 M $(NH_4)_2SO_4$	(27)
4H0D	Ampicillin	1.5	4.48/4.49	2.08/2.09	2.79/2.79	0.2 M NaCl, 0.1 M HEPES pH 7.5, 25 % w/v PEG 3350, 10 mM **$MnCl_2$**	(23)
4HL2	Ampicillin	1.05	4.60/4.60	1.94/1.96	3.04/3.04	0.2 M $(NH_4)_2SO_4$, 0.1 M Bis-Tris pH 5.5, 25% PEG 3350, 100 mM ampicillin	(23)
4RAW	Ampicillin	1.3	4.59/4.60	2.05/2.07	2.98/2.97	0.2 M NaCl, 0.1 M Tris pH 7.0, 30% PEG 3000, 5 mM $CdCl_2$, 200mg/ml ampicillin	Cd1-Cd2 at active site M67V
4RL0	Cefuroxime	1.3	3.81/3.83	2.01/2.03	2.16/2.17	30% PEG3350, 0.1M Bis-Tris pH 6.0, 0.2 M Li_2SO_4	(27), C8 Coo^- did not coordinate to zn1
4EYL	Meropenem	1.9	4.05/3.88	-	-	1M trisodium cacodylate, 0.1M sodium cacodylate pH 6.5	(22), C7 Coo^- intercalates between two Zn ions
5N0H	Meropenem	1.9	4.01/3.83	2.04/2.08	2.66/2.15	1M trisodium cacodylate, 0.1M sodium cacodylate, pH 6.5	Intercalate between two Zn ions
4RBS	Meropenem	2.4	4.00/4.00	-	-	2.8 M sodium acetate pH 7.0	C3 Coo^- did not coordinate to Zn2
5YPK	Imepenem	2.0	3.87~4.15	-	-	28% (w/v) PEG 3350, 0.1M Bis-Tris, pH 5.8, 0.2M ammonium sulfate	(29), EI2
5YPI	Imepenem	2.3	4.03~4.25	-	-	28% (w/v) PEG 3350, 0.1M Bis-Tris, pH 5.8, 0.2M ammonium sulfate	(29), EI1
5YPL	Imepenem	1.8	3.89/3.86	-	-	28% (w/v) PEG 3350, 0.1M Bis-Tris, pH 5.8, 0.2M ammonium sulfate	(29), EP, intercalation
5YPM	Meropenem	2.15	3.93~4.30	-	-	28% (w/v) PEG 3350, 0.1M Bis-Tris, pH 5.8, 0.2M ammonium sulfate	(29), EI1
5YPN	Meropenem	2.12	4.08/4.31	-	-	28% (w/v) PEG 3350, 0.1M Bis-Tris, pH 5.8, 0.2M ammonium sulfate	(29), EI2

637

638

639 **Table 2.** Active site conformations of native NDM-1 structures

PDB	Remark	Resolution (Å)	M1-M2 distance (Å)	M1-OH distance (Å)	OH-M2 distance (Å)	Coordinate error (Å)	Reference
5XP6	native, form 1 Succinate pH5.5	0.95	3.95	1.92	2.55	0.009	This work
5ZGI	native, form 1 Succinate pH6.5	0.98	3.78	1.93	2.35	0.011	This work
5ZGX	native, form 1 Succinate pH7.5	0.95	3.59	1.96	2.09	0.010	This work
5ZGW	native, form 1 Succinate pH7.5 (back soaked from pH5.5)	0.95	3.53	1.97	2.02	0.011	This work
5ZGF	Q123G, form1 Succinate pH7.5	1.20	**3.84**	1.90	**2.43**	0.029	This work
5ZGZ	native, form 1 Imidazole pH7.5	0.95	3.62	1.98	2.04	0.011	This work
5ZGY	native, form 1 Bis-Tris pH7.5	0.95	3.49	1.96	2.00	0.011	This work
5ZGU	native, form 2 HEPES pH7.0	1.55	3.43/3.42	2.11/2.11	2.13/2.12	0.049	This work
5ZGT	native, form 2 HEPES pH7.5	1.20	3.42/3.39	2.05/2.04	2.07/2.05	0.020	This work
5ZH1	native, form2 Imidazole pH7.5	1.05	3.41/3.42	1.93/1.95	1.96/1.95	0.022	This work
5ZGV	native, form2 Tris pH8.0	1.15	3.43/3.40	2.052.06	2.06/2.07	0.021	This work
3SPU	Amonium sulfate pH8.5	2.1	3.84/3.88/3.97/ 3.84/3.56	2.54/1.93/2.11/ 2.08/1.98	2.46/2.60/2.20/ 2.37/2.09		(18)
3ZR9	Zn-Cd pH7.5	1.91	3.64	1.93	2.38		(20)
5JQJ	Mutant, $MgSO_4$ pH6.75	1.67	3.61	1.89	2.21		
4TZE	NDM-5 pH7.5	1.57	3.49/3.56	2.05/2.05	2.07/2.07		
4TZF	NDM-8 Bis-Tris pH5.5	1.22	3.70	2.00	2.13		
4TYF	NDM-4 pH7	1.10	3.54	1.89	2.03		
4RM5	D124N Tris pH7.5	2.1	4.01/4/.10/4.10/ 4.11	2.61/2.53/2.85/ 2.58	2.60/2.72/2.72/ 2.57		(27)

640

641 Table 3 Enzymatic characterization of wild type and mutant NDM-1using imipenem as

642 substrate

	WT(pH5.5) succinate	WT(pH6.5) succinate	WT(pH7.5) succinate	WT(pH7.5) HEPES	A121F(pH7.5) HEPES	Q123G(pH7.5) HEPES
Kcat (s^{-1})	1283±85	2060±245	3960±160	1815±104	221±5.6	686±38
K_M (μM)	337±44	523±103	1415±72	560±52	55±4.6	201±28
Kcat/K_M (M^{-1} s^{-1})	3.82×10^6	3.94×10^6	2.80×10^6	3.24×10^6	4.02×10^6	3.41×10^6

643